



OPEN ACCESS

EDITED BY
Defang Li,
Binzhou Medical University, China

REVIEWED BY
Gaurav Kandoi,
Invaio Sciences, United States
Xinwei Huang,
Tongji University, China

*CORRESPONDENCE
Xiaochang Ma,
maxiaochang@x263.net

SPECIALTY SECTION
This article was submitted to
Cardiovascular and Smooth Muscle
Pharmacology,
a section of the journal
Frontiers in Pharmacology

RECEIVED 27 July 2022
ACCEPTED 06 September 2022
PUBLISHED 26 September 2022

CITATION
Wang A, Zhao W, Yan K, Guo L, Gao F,
Chen J, Wang Y and Ma X (2022),
Investigating the cardioprotective
effects of Fuzheng Yangxin recipe based
on network pharmacology and
experimental evaluation.
Front. Pharmacol. 13:1004929.
doi: 10.3389/fphar.2022.1004929

COPYRIGHT
© 2022 Wang, Zhao, Yan, Guo, Gao,
Chen, Wang and Ma. This is an open-
access article distributed under the
terms of the [Creative Commons
Attribution License \(CC BY\)](https://creativecommons.org/licenses/by/4.0/). The use,
distribution or reproduction in other
forums is permitted, provided the
original author(s) and the copyright
owner(s) are credited and that the
original publication in this journal is
cited, in accordance with accepted
academic practice. No use, distribution
or reproduction is permitted which does
not comply with these terms.

Investigating the cardioprotective effects of Fuzheng Yangxin recipe based on network pharmacology and experimental evaluation

Anzhu Wang^{1,2}, Wei Zhao³, Kaituo Yan³, Lijun Guo^{1,4},
Feng Gao^{1,2}, Jingjing Chen^{1,2}, Yifei Wang^{1,5} and
Xiaochang Ma^{1,4*}

¹Xiyuan Hospital, China Academy of Chinese Medical Sciences, Beijing, China, ²Graduate School, China Academy of Chinese Medical Sciences, Beijing, China, ³Yidu Central Hospital of Weifang, Weifang, China, ⁴National Clinical Research Center for Chinese Medicine Cardiology, Beijing, China, ⁵Beijing University of Chinese Medicine, Beijing, China

Background: Under Chinese medicine theory guidance, Fuzheng Yangxin Recipe (FZYX) is clinically effective for the treatment of heart failure (HF) caused by ischemic heart disease (IHD). This study aimed to investigate the mechanism of the myocardial protective effects of FZYX on HF.

Materials and methods: The Gene expression omnibus database was used to identify differential genes of the IHD subtype. Through network pharmacological methods, the targets of the active components of FZYX were obtained. We also constructed IHD-induced HF model rats by ligating the left anterior descending coronary artery. Echocardiography, pathological section staining, enzyme-linked immunosorbent assay, western blotting, immunohistochemistry, and quantitative real-time PCR analyses were performed to verify the protective effects of FZYX on the myocardium.

Results: We identified 53 active components and 37 potential targets of FZYX associated with the IHD subtype. Signal transducer and activator of transcription 3 (STAT3) is a key protein in the protein-protein interaction (PPI) network. A total of 146 biological processes, 10 cellular components and 40 molecular function subcategories were identified by Gene Ontology (GO) enrichment analysis, and 18 signalling pathways, including apoptosis, were identified by Kyoto Encyclopedia of Genes and Genomes (KEGG) enrichment analysis. *In vivo* experiments showed that FZYX significantly inhibited cardiomyocyte apoptosis, promoted the expression and phosphorylation of STAT3, and improved cardiac function.

Conclusion: FZYX improves cardiac function and protects cardiomyocytes from injury via multi-component, multi-target and multi-pathway action, especially its possible role in regulating STAT3 expression and anti-apoptotic effect.

KEYWORDS

ischemic heart disease, heart failure, Fuzheng Yangxin recipe, network pharmacology, bioinformatics analysis, experimental verification

1 Introduction

Heart failure (HF) is one of the main public health problems worldwide. In the 2017 Global Burden of Disease Study, the number of HF patients was 64.34 million (Disease, 2018). Data from the USA in 2019 showed that 6.2 million people aged >20 years suffered HF, and HF-associated morbidity is estimated to increase by 46% from 2012 to 2030 (Benjamin et al., 2019). Ischemic heart disease (IHD) is an important cause of HF, and acute myocardial infarction (MI) is often the first manifestation. The China-HF Registry indicates that patients with HF and coronary heart disease account for 49.6% (Zhang et al., 2017). With the advancement of medical treatment, the morbidity of HF following MI has decreased, but the mortality is still high. A SWEDEHEART study involving 199,851 cases of acute MI showed that the incidence of HF after acute MI dropped from 46% in 1996 to 28% in 2008. However, the 1-year mortality after HF only dropped from 36% in 1996 to 31% in 2008, which is higher than in non-HF patients (Desta et al., 2015). This is because although reperfusion therapy can save the ischemic myocardium caused by infarction, it can also induce other irreversible damage such as cardiomyocyte necrosis and coronary microvascular dysfunction, which may aggravate ventricular remodelling (Heusch, 2020). Therefore, drug treatment of HF caused by IHD is a major research focus.

HF is not mentioned in traditional Chinese medicine (TCM), but its clinical symptoms were described more than 2000 years ago. Chinese medicine proposes that the onset of HF is related to impairment of the “Yangqi” in the heart, and herbal medicine is widely used in the treatment of patients with HF in China (Tang and Huang, 2013). Fuzheng Yangxin Recipe (FZYX) is a TCM concoction consisting of 6 g of *Panax notoginseng* (Burkill) F. H. Chen, 20 g of *Panax ginseng* C. A. Meyer, 30 g of *Rhodiola crenulata* (Hook.f. et Thoms.) H. Ohba, 10 g of *Aconitum carmichaeli* Debx, 20 g of *Ophiopogon japonicus* (Linn. f.) Ker-Gawl, 30 g of *Astragalus membranaceus* (Fisch.) Bunge, 15 g of *Angelica sinensis* (Oliv.) Diels and 15 g of *Rehmannia glutinosa* Libosch. In clinical practice, FZYX has a beneficial effect on patients with HF caused by IHD (Guo, 2018; Zheng, 2020), but the underlying mechanism remains unclear.

Network pharmacology, based on systems biology and multi-directional pharmacology, allows the selection of specific nodes using biomolecular network analysis methods to carry out molecular design and target analysis of drugs (Gosak et al., 2018). This method is dynamic, systemic and interactive, and can construct a ‘disease-gene-target-component-drug’ network from the perspective of systems biology, which is highly coincident with the holistic concept, and syndrome differentiation and treatment of TCM (Kibble et al., 2015). The

present study explored the mechanism of FZYX in the treatment of HF based on network pharmacology, including *in vivo* experiments. The findings provide a foundation for the treatment of HF by FZYX.

2 Materials and methods

2.1 Gene chip analysis and identification of differentially expressed genes based on the gene expression omnibus

Firstly, we retrieved HF gene expression profiles and selected “Homo sapiens” entries from the gene expression omnibus (GEO) database. After reading the abstract, we selected entries according to the following criteria: 1) The number of samples was >40 (>20 for both experimental and control groups); 2) Healthy people were used as the control group; 3) Clinical samples were myocardial tissue. Secondly, Matrix and Platforms were downloaded after targets were selected, and the R packages BiocManager, Limma and Pheatmap were used to perform a secondary analysis of the chip data, with $|\log_2FC$ (fold change) > 0.5 and $adjPvalue < 0.05$ as the cut-off criteria for differentially expressed genes (DEGs). Finally, we selected the top 20 genes with the highest up- and downregulation to draw a heatmap. Genes unaffected and differential genes were used to draw a volcano map.

2.2 Fuzheng Yangxin Recipe active ingredient screening and target prediction

The BATMAN-TCM database (Liu et al., 2016) and the ETCM database (Xu et al., 2019) were used to screen effective ingredients for each TCM concoction, with adjusted p -value = 0.05 and score cutoff = 20 when using the BATMAN-TCM database, and Druglikeness Grading = ‘Moderate’ or ‘Good’ when using the ETCM database. The obtained components were used by the SwissTargetPrediction database (<http://www.swisstargetprediction.ch/>) to predict targets, which were organised into a table according to herb-ingredient code-ingredient name-target.

2.3 Construction of a traditional Chinese medicine compound regulatory network

DEGs in Section 2.1 and target genes of FZYX identified in Section 2.2 were used to draw a Venn diagram, and Cytoscape

(Version 3.8.2) was used to construct a regulatory network of herb components with the names, intersecting genes, and active ingredients of medicines as nodes (Shannon et al., 2003).

2.4 Construction of a protein-protein interaction network

Researchers used “BisoGenet” in Cytoscape and data from six major human PPI databases (BioGRID, BIND, MINT, HPRD, DIP and intAct) to perform PPI network analysis of overlapping genes (Martin et al., 2010). The CytoNCA plug-in was used to carry out network topology analysis and to set degree centrality (DC) $\geq 20\%$ and between centrality (BC) $\geq 20\%$ as the core node screening conditions. Key nodes were important proteins in drug-target-gene information transmission.

2.5 Functional enrichment analysis

Gene Ontology (GO) provides functional annotation for biological process (BP), cellular component (CC) and molecular function (MF) categories. The Kyoto Encyclopedia of Genes and Genomes (KEGG) database was applied to analyse the signalling pathways in which the differential genes are involved. The R packages org.Hs.eg.db, DOSE, clusterProfiler, enrichplot, colorspace, stringi and ggplot2 can be used for visualisation of GO and KEGG results. According to the value and significance of enrichment (p -value cut-off < 0.05 , q -value cut-off < 0.05), a bubble diagram was generated, KEGG pathways were imported into Cytoscape, and a pathway-gene network was drawn based on degree values.

2.6 Molecular docking

The intersection of key nodes in the PPI network and high relevance genes in pathway-gene network were selected as candidate genes for molecular docking. The receptors 3D format of the core targets were downloaded from the Protein Data Bank (<https://www.rcsb.org/>) (Burley et al., 2021), and operations including dehydration, hydrogenation and ligand extraction were performed using Pymol 2.5 software (Mooers, 2020). Autodock Vina 1.1.2 software was used for molecular docking (Trott and Olson, 2010).

2.7 Medicine preparation

Panax notoginseng (Burkill) F. H. Chen (60100000994), *Panax ginseng* C. A. Meyer (60100000951), *Rhodiola crenulata* (Hook.f. et Thoms.) H. Ohba (SA200226005), *Aconitum carmichaeli* Debx (SA200325013), *Ophiopogon japonicus* (Linn.

f.) Ker-Gawl (60100000925), *Astragalus membranaceus* (Fisch.) Bunge (60100000921), *Angelica sinensis* (Oliv.) Diels (SA200530014) and *Rehmannia glutinosa* Libosch (60100000919) were purchased from China Resources Sanjiu (Beijing, China). In addition, angiotensin receptor neprilysin inhibitors (ARNI) were purchased from Novartis (SDC563, Beijing, China) and employed as positive control drugs.

2.8 Establishment of an myocardial infarction rat model and groupings

This experiment included 40 specific pathogen free male Sprague Dawley rats weighing 200 ± 20 g purchased from Charles River (SYXK 2018-0018, Beijing, China). Animals were raised in the experimental animal room of Xiyuan Hospital. Standard synthetic feed was provided with free access to drinking pure water, the temperature was $(24 \pm 2^\circ\text{C})$, the humidity was 45%–50%, and a 12 h/12 h light/dark photoperiod was employed. Animal experiments were reviewed and approved by the ethics committee of Xiyuan Hospital. Rats were randomly divided into four groups; a sham operation group, a model group, an FZYX group (4.2 g/kg) and an ARNI (68 mg/kg) group. Animal drug dosage was based on the equivalent conversion between body surface area and weight of animals and humans (Huang et al., 2004), as well as previous related studies (Pfau et al., 2019; Vaskova et al., 2020). Rats in the sham operation and model groups were intragastric with equal amounts of phosphate-buffered saline (PBS). The drug was administered continuously for 42 days (Gan et al., 2014; Sunagawa et al., 2014; Wang et al., 2020).

MI-induced HF model rats were established by ligating the left anterior descending coronary artery. Briefly, rats were intubated following being anesthetised with 1% sodium pentobarbital (50 mg/kg intraperitoneal injection) using an ALC-V8S-P small animal ventilator (Alcott Biotech, Shanghai, China) at a rate of 70 breaths per min, ribs were separated to expose the heart, and a 4/0 medical silk thread was employed to ligate the artery 2–3 mm below the left atrial appendage. If the electrocardiogram indicated ST-segment elevation and the colour of the ligation area was immediately pale, ligation was considered successful (Lindsey et al., 2018). In the sham operation group, rats were threaded but arterial ligation was not performed.

2.9 Echocardiography assessment

After rats were fed drugs for 42 days, uninformed researchers anesthetized them with 1% sodium pentobarbital (50 mg/kg), and two-dimensional M-mode and B-mode echocardiography were performed using a Vevo2100 instrument (Visualsonics, Toronto, Canada) to assess left ventricular function. The left

TABLE 1 Antibodies used in western blotting.

Protein	Antibody	Concentration
BCL-2	Anti-BCL-2 (bs-20351R, Bioss)	1 µg/ml
BAX	Anti-BAX antibody (bs-4564R, Bioss)	1 µg/ml
Caspase-3	Anti-cleaved caspase-3 (ab2302, Abcam)	0.5 µg/ml
pSTAT3	Anti-phospho-STAT3 (Tyr705) (bs-1658R, Bioss)	2 µg/ml
STAT3	Anti-STAT3 (bs-20382R, Bioss)	2 µg/ml
GAPDH	Anti-GAPDH (bs-0755R, Bioss)	1 µg/ml
	Goat anti-rabbit IgG H&L/HRP second antibody (bs-40295G-HRP, Bioss)	2 µg/ml

ventricular ejection fraction (LVEF), left ventricular fractional shortening (LVFS), left ventricular end-diastolic volume (LVEDV), left ventricular end-systolic volume (LVESV), left ventricular internal dimension end-diastolic (LVIDd) and left ventricular internal dimension end-systolic (LVIDs) were automatically calculated by the echocardiographic system.

2.10 Pathological section staining

Heart tissue of rats fed drugs for 42 days was collected and fixed in 4% paraformaldehyde overnight. Myocardial tissue was embedded and fixed in paraffin to prepare 4 µm sections. Different concentrations of ethanol were used for dewaxing, and samples were stained using a modified Masson's Trichrome Stain Kit (G1346, Solarbio, Beijing, China) and a hematoxylin-eosin (HE) Staining Kit (G1120, Solarbio). Finally, myocardial tissue morphology and fibrosis degree were observed under a 400× microscope. Collagen volume fraction (CVF) was analyzed by Image-Pro Plus 6.0 (Media Cybernetics, Inc., Rockville, Maryland, United States). $CVF = \text{area of collagen} / \text{total area} \times 100\%$.

2.11 Enzyme-linked immunosorbent assay

Blood was collected from the abdominal aorta, incubated at room temperature for 1 h, then centrifuged at 1000 g for 10 min at 4°C. Enzyme-linked immunosorbent assay (ELISA) was employed to determine the level of N-terminal pro-B-type natriuretic peptide (NT-proBNP; AD2817Ra, Andygene, Beijing, China) according to the manufacturer's instructions.

2.12 Western blotting

The infarction border area of the left ventricular myocardium was rapidly frozen in liquid nitrogen. The RIPA buffer (R0020, Solarbio) was added, the tissue was homogenised on ice, then centrifuged at a low temperature to extract total protein. Protein

concentration was measured using a bicinchoninic acid (BCA) protein assay kit (AR1189, Boster, Wuhan, China). Equal amounts of proteins (50 µg) were separated based on molecular weight by 8%–12% sodium dodecyl sulphate polyacrylamide gel electrophoresis (SDS-PAGE), then transferred to a polyvinylidene fluoride (PVDF) membrane. Membranes were blocked with quick block buffer for western blot (P1623, Applygen, Beijing, China) at room temperature and incubated overnight at 4°C in the presence of primary antibody (Table 1). The membranes were washed three times with Tris Buffered Saline with Tween 20 (TBST), then incubated with the secondary antibody at room temperature for 1 h. The membrane was then developed using a western blotting 3,3'-diaminobenzidine (DAB) Chromogenic Assay Kit (SA2025, Boster), and bands were analysed using Image J software (Schneider et al., 2012).

2.13 Immunohistochemistry

Tissue sections were dewaxed and rehydrated, then subjected to antigen repair using the citric acid solution (pH 6.0). Hydrogen peroxide (3%) was used to block sections for 10 min, and 5% goat serum (SL038, Solarbio) was added and incubated for 1 h. Tissue sections were incubated with primary antibody (cleaved Caspase-3, 2 µg/ml, ab2302, Abcam, Cambridge, Massachusetts, United States) overnight at 4°C, followed by secondary antibody (3 µg/ml, bs-40295G-HRP, Bioss, Beijing, China). Finally, immunohistochemical reactions were analysed using a DAB Kit (AR1022, Boster) and nuclei were stained with HE (G1080, Solarbio). Images were observed under a microscope at 400× magnification. The integrated option density (IOD)/area was analysed using Image-Pro Plus 6.0.

2.14 Quantitative real-time PCR

RNA was extracted from the infarction border area of the left ventricular myocardium according to the instructions supplied with the Total RNA Extraction Kit (DP419, Tiangen, Beijing,

TABLE 2 Primer sequences for each gene.

Gene	Primer sequence (5'→3')	Temp (°C)
BCL-2	Forward: GGTGAACTGGGGGAGGATTG	Forward: 60.03
	Reverse: AGAGCGATGTGTCCACCAG	Reverse: 60.02
BAX	Forward: CACGTCTGCGGGGAGTCA	Forward: 61.68
	Reverse: TAGGAAAGGAGGCCATCCCA	Reverse: 59.95
Caspase-3	Forward: GAGCTTGAACGCGAAGAAA	Forward: 59.13
	Reverse: TAACCGGGTGC GG TAGAGTA	Reverse: 60.03
STAT3	Forward: CTGAGGTACAATCCCGCTCG	Forward: 60.25
	Reverse: TCGGTCAGTGTCTTCTGCAC	Reverse: 59.97
GAPDH	Forward: GCATCTTCTTGTGCAGTGCC	Forward: 60.11
	Reverse: GATGGTGATGGGTTTCCCGT	Reverse: 60.03

China). The PrimeScript RT reagent Kit (RR037A, TaKaRa Bio, Beijing, China) was used for reverse transcription of RNA samples into cDNA. Primer sequences are listed (Table 2). Each 20 μ l contained 6.8 μ l of diethyl pyrocarbonate (DEPC) water, 100 μ l of THUNDERBIRD SYBR qPCR Mix (QPS-201, Toyobo, Shanghai, China), 0.6 μ l of forward primer, 0.6 μ l of reverse primer, and 2 μ l of cDNA. Thermal cycling involved an initial denaturation step at 95°C for 10 min, followed by 40 cycles at 95°C for 10 s, 55–60°C for 30 s, and 72°C for 10 s. The expression level of each gene was calculated using the $2^{-\Delta\Delta CT}$ method (Chen et al., 2021).

2.15 Statistical analysis

Data were statistically analysed by SPSS Statistics software (Version 25, IBM Corp., Armonk, New York, United States). All data are presented as mean \pm standard deviation. One-way analysis of variance (ANOVA) with a completely random design was used for comparison between multiple groups, and the least significant difference (LSD) test was used for pairwise comparison between groups. When applying one-way ANOVA was not appropriate, the Kruskal-Wallis rank sum test was used. A p -value <0.05 was considered statistically significant.

3 Results

3.1 Differentially expressed genes analysis of heart failure based on the gene expression omnibus database

The GSE57338 chip and platform files from the GEO database were downloaded to obtain sample data from 136 non-failing (NF), 95 IHD with HF and 82 idiopathic dilated cardiomyopathy (DCM) with HF. To gain a better understanding of the different HF subtypes, we performed

differential expression analysis on all types of HF patients based on the data. The patients' characteristics (age and sex) were shown in Table 3. R software and related packages were used to filter and standardise the data and screen DEGs. In total, 420 DEGs between NF and IHD (238 upregulated and 182 downregulated) were identified, and the top 20 genes with the most significant upregulation and downregulation were plotted in a heatmap and the top 10 genes with the most significant upregulation and downregulation were marked in a volcano map (Figure 1A). 459 DEGs between NF and DCM (248 upregulated and 211 downregulated) were identified, and the top 20 genes with the most significant upregulation and downregulation were plotted in a heatmap and the top 10 genes with the most significant upregulation and downregulation were marked in a volcano map (Figure 1B). USP9Y and VSIG4 were found to be specifically expressed in IHD, while SMOC2 and CYP4B1 were discovered to be uniquely expressed in DCM. (Figures 1C–E). The DEGs are available in Supplementary Table S1.

3.2 Fuzheng Yangxin Recipe components and targets

Components were identified by database screening, including 23 ingredients in *Panax notoginseng* (Burkill) F. H. Chen, 43 in *Panax ginseng* C. A. Meyer, 4 in *Rhodiola crenulata* (Hook.f.et Thoms.) H. Ohba, 8 in *Aconitum carmichaeli* Debx, 27 in *Ophiopogon japonicus* (Linn. f.) Ker-Gawl, 2 in *Astragalus membranaceus* (Fisch.) Bunge, 47 in *Angelica sinensis* (Oliv.) Diels and 4 in *Rehmannia glutinosa* Libosch. After deduplication, 405 components were identified in FZYX. In addition, targets were identified by database screening, including 369 ingredients in *Panax notoginseng* (Burkill) F. H. Chen, 423 in *Panax ginseng* C. A. Meyer, 124 in *Rhodiola crenulata* (Hook.f.et Thoms. H. Ohba, 44 in *Aconitum carmichaeli* Debx, 473 in *Ophiopogon japonicus* (Linn. f.) Ker-Gawl, 180 in *Astragalus membranaceus* (Fisch.) Bunge, 591 in *Angelica sinensis* (Oliv.) Diels and 77 in *Rehmannia glutinosa* Libosch. After deduplication, 923 targets in FZYX were identified (Supplementary Table S2).

3.3 Drug-disease intersection genes and herbal compound regulatory network analysis

Target genes of FZYX were intersected with disease-related genes, and 37 intersection genes were obtained (Figure 1E). These intersection genes are potential targets of FZYX in the treatment of IHD-induced HF. An ingredient-intersection gene regulatory network diagram of FZYX was constructed with Cytoscape 3.8.2 software, containing 90 nodes (37 genes, 53 ingredients)

TABLE 3 Characteristics of patients.

Characteristics	IHD, <i>n</i> = 95	DCM, <i>n</i> = 82	Non-failing, <i>n</i> = 136
Gender, No. (%)			
Male	81 (85.26%)	63 (76.83%)	73 (53.68%)
Female	14 (14.74%)	19 (23.17%)	63 (46.32%)
Age			
Years (mean ± SD)	59.11 ± 7.39	51.16 ± 13.98	49.36 ± 15.00

and 182 edges (Figure 2A). Links between nodes represent the functional relationships of these nodes, and the greater the number of connected nodes, the more important the role of the target or ingredient in the network. Analyse-Network was used to calculate the network degree, and ingredients with higher degrees included Gomisin A, Kumatakenin, Methylophipogonanone B and Senkyunolide A (Supplementary Table S3).

3.4 Topological analysis of the protein-protein interaction network

Researchers used BisoGenet to construct a PPI network of 37 intersection genes, which includes 1,260 nodes and 18,091 edges (Supplementary Table S4); the final 29 key nodes and 243 edges were obtained by screening with the CytoNCA software package. Based on the core network, signal transducer and activator of transcription 3 (STAT3) was identified as the key protein in the PPI core network (Figure 2B).

3.5 Gene ontology functional analysis

To further understand the mechanism of FZYX, GO and KEGG were performed. GO functional analysis was performed on 37 key intersection genes with $p < 0.05$. The final enrichment results comprised 1) 146 BP subcategories including vascular-associated smooth muscle contraction, extracellular matrix disassembly, positive regulation of cytosolic calcium ion concentration, regulation of lipase activity, regulation of protein serine/threonine kinase activity, regulation of inflammatory response, and collagen catabolic process; 2) 10 CC subcategories including nuclear membrane, external side of plasma membrane and nuclear envelope; 3) 40 MF subcategories including protease binding, endopeptidase activity, phosphoric diester hydrolase activity, exopeptidase activity and phospholipase activity. The top 20 BP and MF subcategories and the top 10 CC subcategories are shown in Figure 3. Details are provided in Supplementary Table S5.

3.6 Kyoto encyclopedia of genes and genomes functional analysis

KEGG pathway analysis showed that 18 signal pathways were enriched (Figure 4A). Based on previous work on the HF mechanism, our results suggest that FZYX may act in HF through the advanced glycation end-product (AGE)-receptor for AGE (RAGE) signalling pathway, arachidonic acid metabolism, the high-affinity receptors for immunoglobulin E (Fc epsilon RI) signalling pathway, the prolactin signalling pathway, nicotinate and nicotinamide metabolism, the forkhead box O (FOXO) signalling pathway, apoptosis, the adipocytokine signalling pathway, the renin-angiotensin system, and the cyclic guanosine monophosphate (cGMP)-protein kinase G (PKG) signalling pathway. Cytoscape was used to construct a “Gene-KEGG signalling pathway” network. The results showed that mitogen-activated protein kinase kinase 1 (MAP2K1), STAT3, cyclin D1 (CCND1) and mitogen-activated protein kinase 10 (MAPK10) were the most enriched genes, suggesting they might be related to the mechanism of FZYX (Figure 4B). Details are provided in Supplementary Table S6.

3.7 Molecular docking

Molecular docking was performed with the main compounds of FZYX and the intersection targets, namely STAT3. The lower the affinity value in the docking findings, the more stable the contact between the targets and the active component was. Through molecular docking, it was found that STAT3 had good binding activities with the active components of FZYX (Table 4). These compounds bind to STAT3 through interacting with various amino acid residues, such as HIS-457, LEU-438, HIS-437, GLN-247, PRO-333, GLU-625, LEU-438 and LYS-370. The binding interactions and the binding sites of compounds-targets were shown in Figure 5. These results suggest that FZYX may act through STAT3.

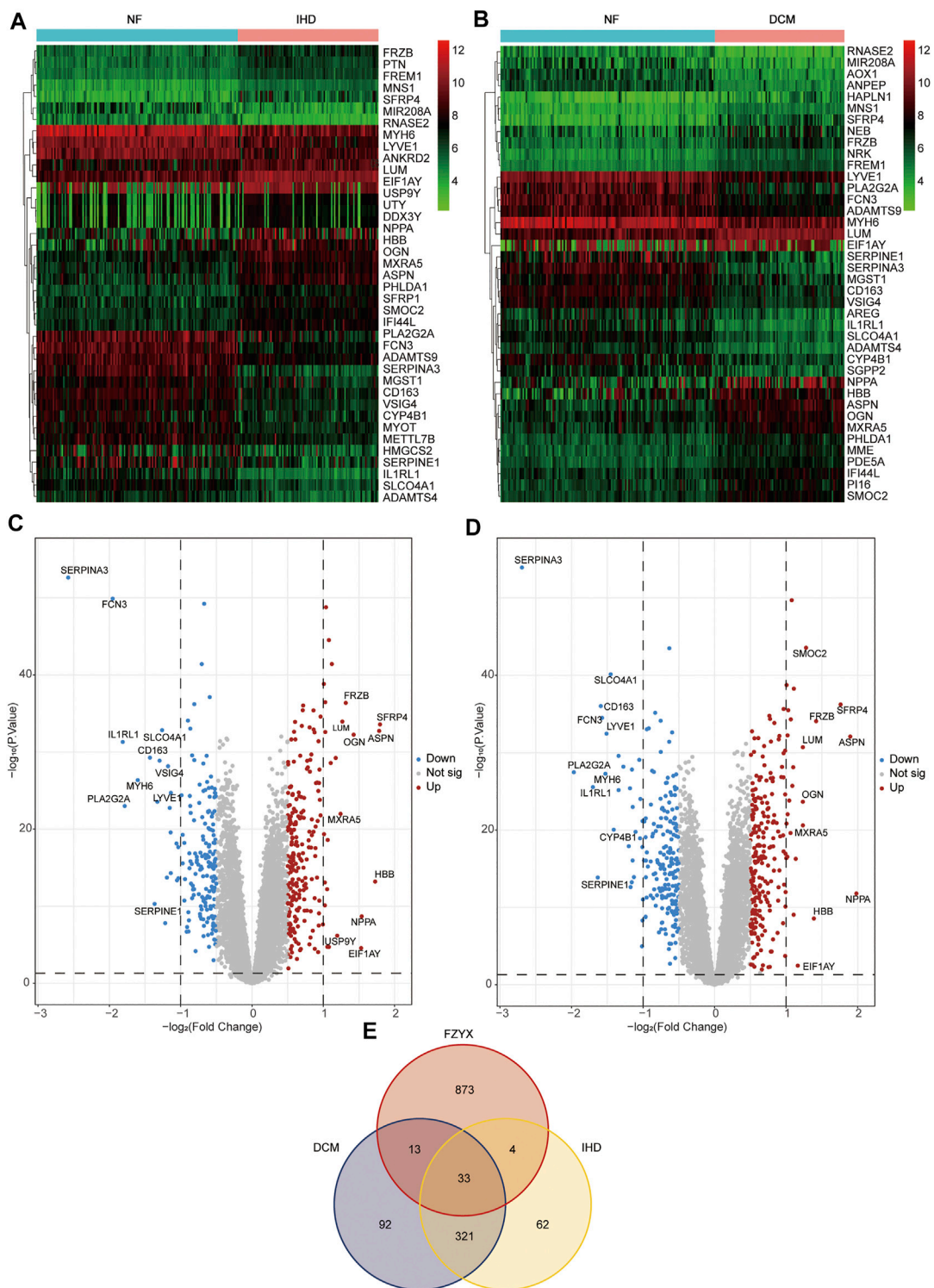


FIGURE 1

Differential gene acquisition and network construction. **(A)** Heatmap of non-failing (NF) vs ischemic heart disease (IHD). Green represents low expression, black represents medium expression, and red represents high expression. **(B)** Heatmap of NF vs idiopathic dilated cardiomyopathy (DCM). Green represents low expression, black represents medium expression, and red represents high expression. **(C)** Volcano map of IHD. **(D)** Volcano map of DCM. **(E)** Venn diagram of FZYX, IHD and DCM.

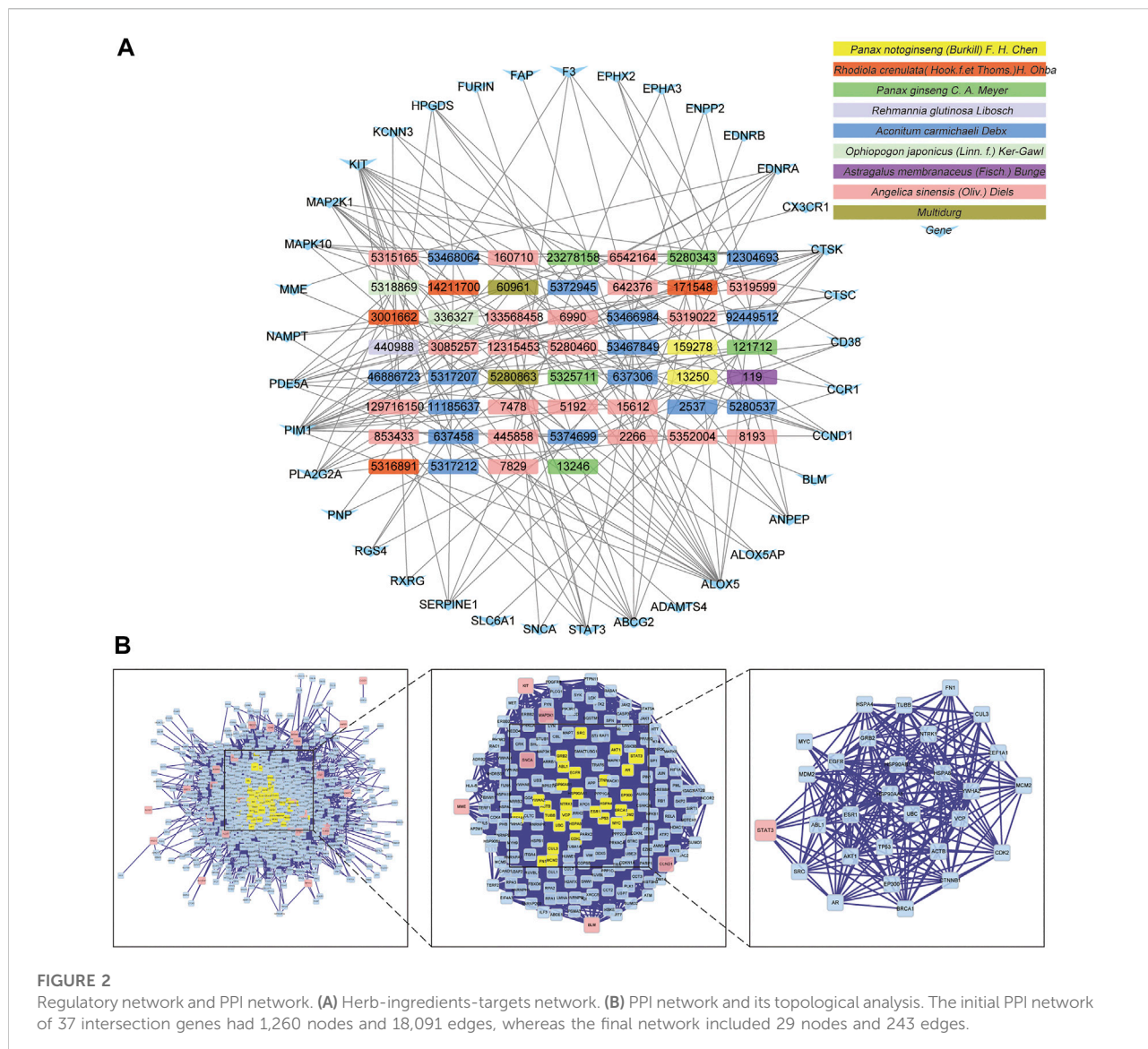
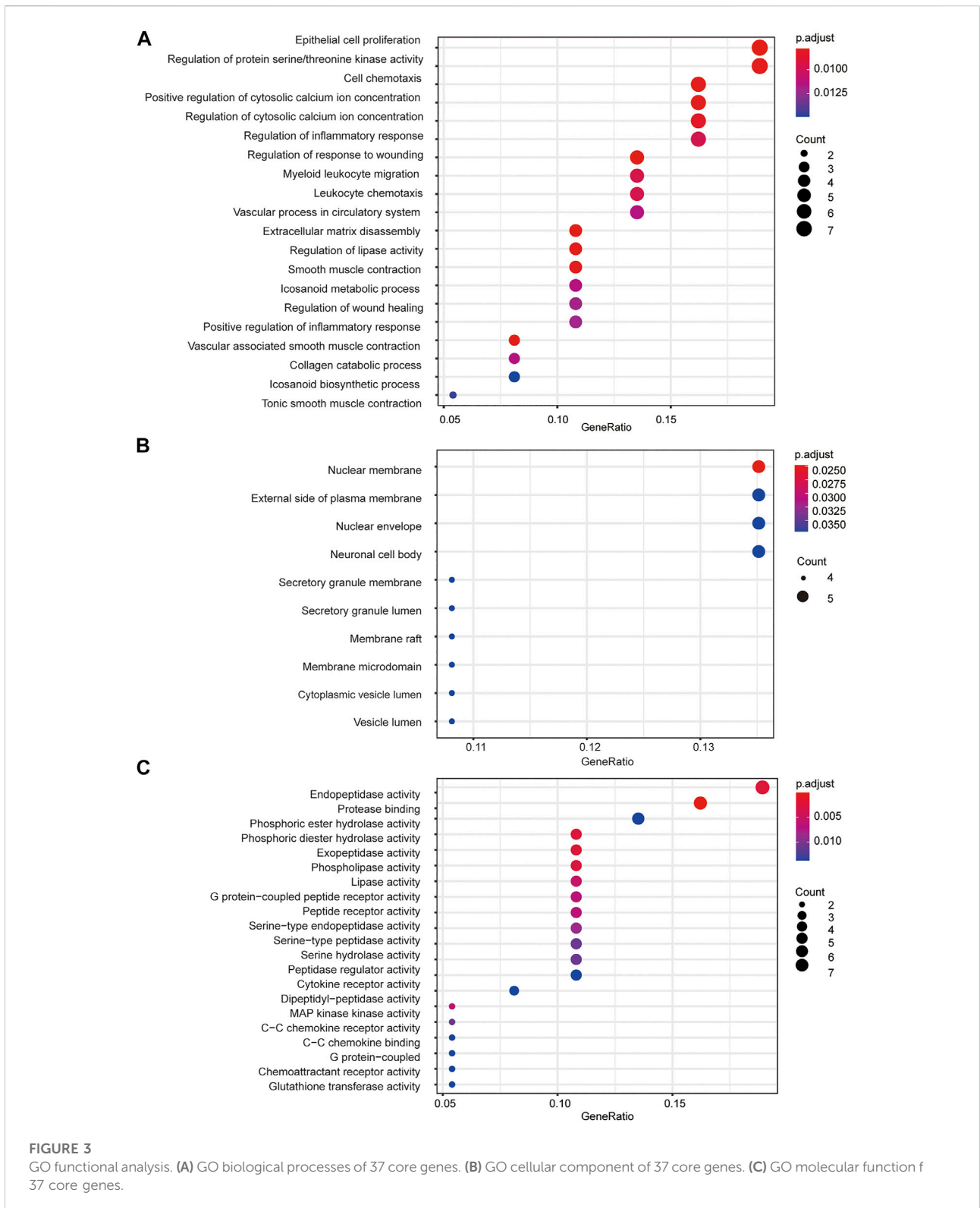


FIGURE 2 Regulatory network and PPI network. (A) Herb-ingredients-targets network. (B) PPI network and its topological analysis. The initial PPI network of 37 intersection genes had 1,260 nodes and 18,091 edges, whereas the final network included 29 nodes and 243 edges.

3.8 Effects of Fuzheng Yangxin Recipe on cardiac function and structural alterations in heart failure model rats

At the end of the experiment cycle, two animals in the model group, one in the FZYX group and none in the remaining groups died. Echocardiographic results showed that LVEF and LVFS were decreased and LVIDs, LVIDd, LVESV and LVEDV were increased in the HF model group compared with the sham operation group, suggesting that cardiac structure and function were severely impaired after acute MI (Figure 6A). LVEF and LVFS were significantly increased and LVIDs, LVIDd, LVESV and LVEDV were significantly decreased after treatment with FZYX (Figure 6A). The HE staining results showed that myocytes

in the sham operation group were structurally intact and well-arranged, while myocytes in the model group were structurally disorganised and loosely arranged. In addition, nuclei in the model group underwent consolidation or fragmentation, and obvious inflammatory infiltration was observed (Figure 6B). A blue collagen fiber distribution in the interstitial space of myocardial cells was evident in the model group following Masson's staining (Figure 6C), and treatment with FZYX significantly improved these pathological changes and CVF significantly decreased (Figure 6E). NT-proBNP is a diagnostic marker of HF (McDonagh et al., 2021). Our results showed that serum NT-proBNP levels were significantly increased in the model group compared with the sham operation group (Figure 6D). After FZYX treatment, all the above indices were significantly decreased, suggesting



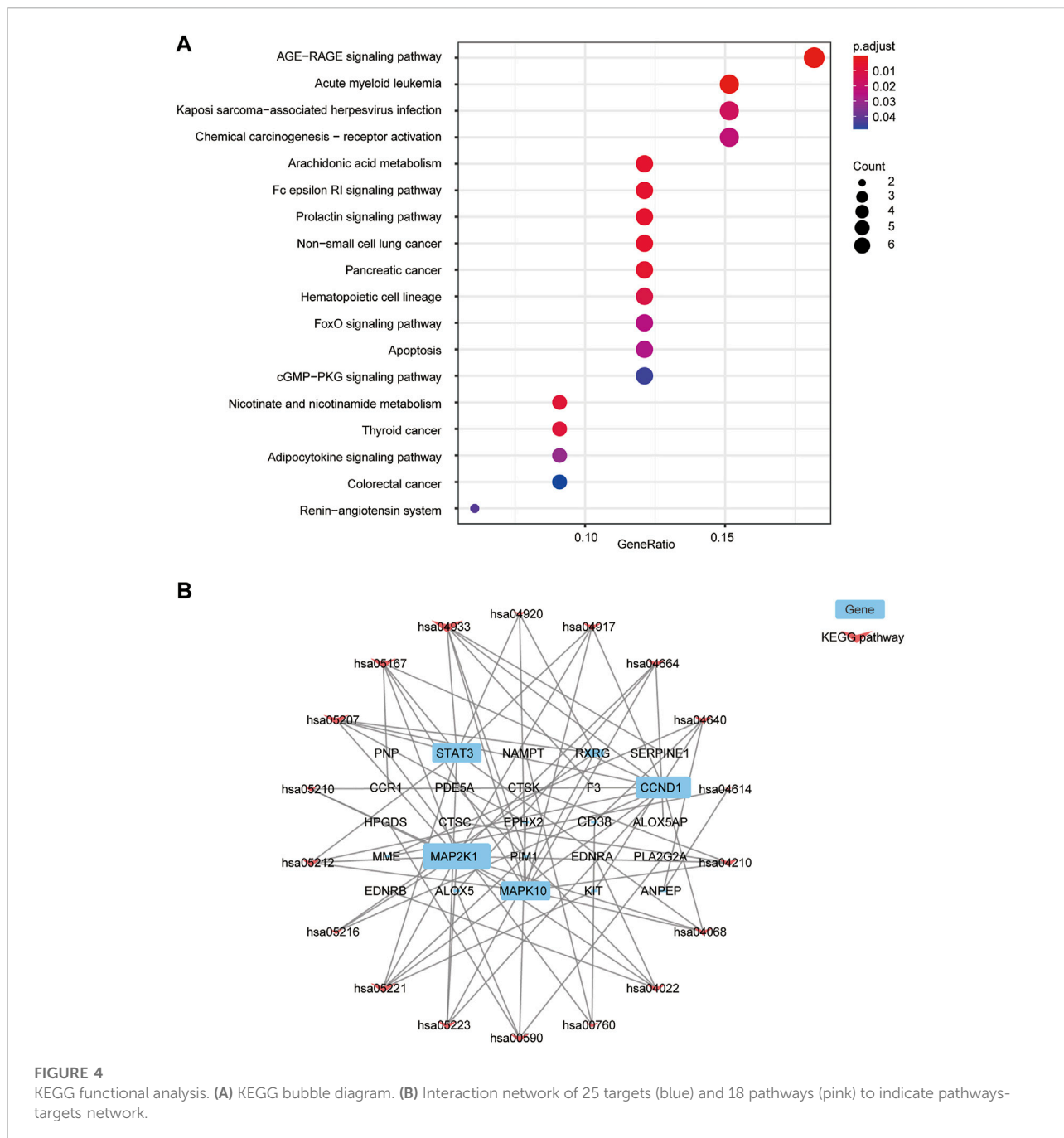


FIGURE 4 KEGG functional analysis. (A) KEGG bubble diagram. (B) Interaction network of 25 targets (blue) and 18 pathways (pink) to indicate pathways-targets network.

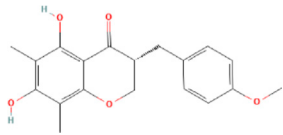
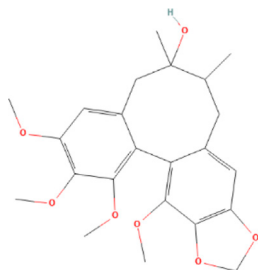
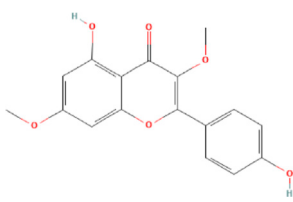
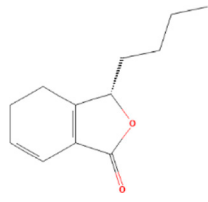
that FZYX protected myocardial structure and cardiac function. The effects of ARNI were similar to those of FZYX.

3.9 Regulation of apoptosis and signal transducer and activator of transcription 3 by Fuzheng Yangxin Recipe

To verify the underlying mechanism of the network pharmacological findings, expression of apoptosis-related

genes at mRNA and protein levels in cardiomyocytes was measured by Quantitative real-time PCR (qRT-PCR) and western blotting, respectively (Figures 7A,B). The results showed that compared with the sham operation group, expression of anti-apoptotic B cell lymphoma-2 (BCL-2), proapoptotic BCL-2 associated X (BAX) and Caspase-3 was significantly increased in the model group. FZYX upregulated the expression of BCL-2 and decreased the expression of BAX and Caspase-3 in HF. Immunohistochemical analysis of Caspase-3 protein was consistent with the above, suggesting that FZYX

TABLE 4 Details of molecular docking.

Component	Structure	PubChem CID	Target	PDB ID	Binding energy (kcal/mol)
Methylophiopogonone B		46886723	STAT3	6NJS	-7.4
Gomisin A		634470	STAT3	6NJS	-6.3
Kumatakenin		5318869	STAT3	6NJS	-6.7
Senkyunolide A		3085257	STAT3	6NJS	-5.6

attenuated cardiac remodelling after MI in rats by inhibiting apoptosis (Figure 7C).

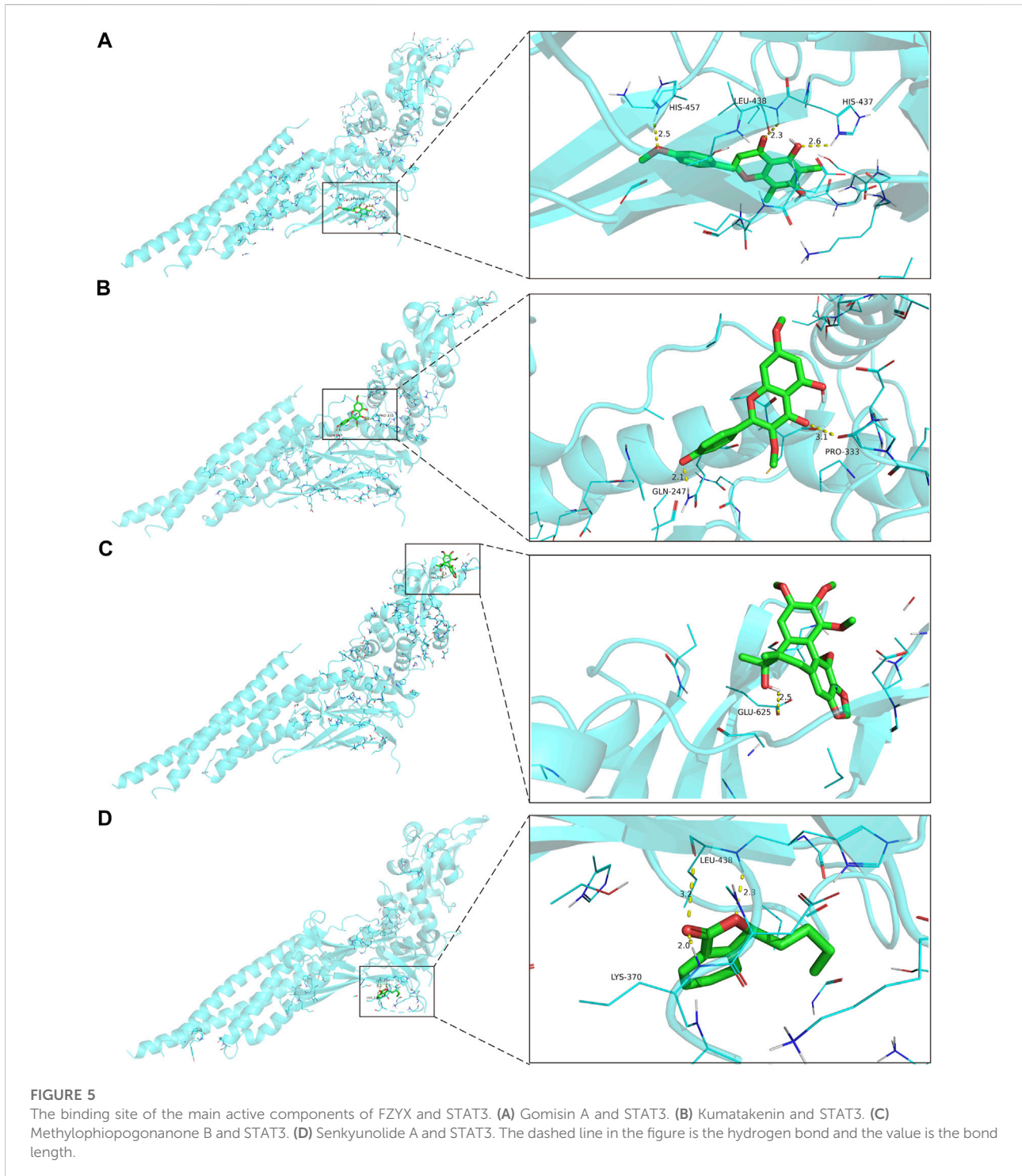
The mRNA expression levels of STAT3 were measured by qRT-PCR, and the abundance of phosphorylated STAT3 and total STAT3 proteins was measured by western blotting according to the results of network pharmacology (Figures 7D,E). Compared with the sham operation group, STAT3 mRNA expression levels were reduced and the pSTAT3/STAT3 ratio was decreased in the model group, while FZYX upregulated STAT3 mRNA levels and protein phosphorylation.

4 Discussion

Based on pattern identification and disease, TCM uses various herb combinations according to conditions to achieve the goal of holistic treatment. Therefore, TCM prescriptions often contain numerous herbs, resulting in complex chemical

composition and numerous targets. Hence, modern research faces great challenges in deciphering their mechanisms and modes of action. Network pharmacology retrieves known chemical components of herbs in prescriptions based on a variety of databases and analysis software. From the data, targets of the chemical components, sites of action, molecules, and pathways can be obtained, allowing comprehensive analysis of the mechanisms of the compounds, and providing a reference for further clinical research on a specific mechanism (Li and Zhang, 2013).

The present study was divided into two parts: network pharmacology and experimental validation. We first used GSE57338 to identify DEGs in HF. GSE57338 includes three groups: NF, IHD and DCM. V-set and immunoglobulin domain containing 4 (VSIG4) is specifically expressed in tissue-resident macrophages and can mediate various cellular events. Inhibition of the expression of VSIG4 can significantly increase the secretion of cytokines in macrophages and aggravate the inflammatory response^[19, 20]. This suggests a strong



relationship between inflammation and IHD, although further validation is needed considering that VSIG4 has been poorly studied in HF. Extracellular matrix changes play an important role in the development of DCM. Different from fibrosis triggered by ischemic conditions, DCM manifests as diffuse fibrosis^[21]. Secreted modular calcium-binding protein

2(SMOC2), as a matrix protein, is a non-structural component of the extracellular matrix^[22]. Whether SMOC2 affects extracellular mechanism components in DCM and plays a key role also needs to be further verified

FZYX has a good clinical effect on IHD-induced HF, but its specific active components are still unclear. We used the

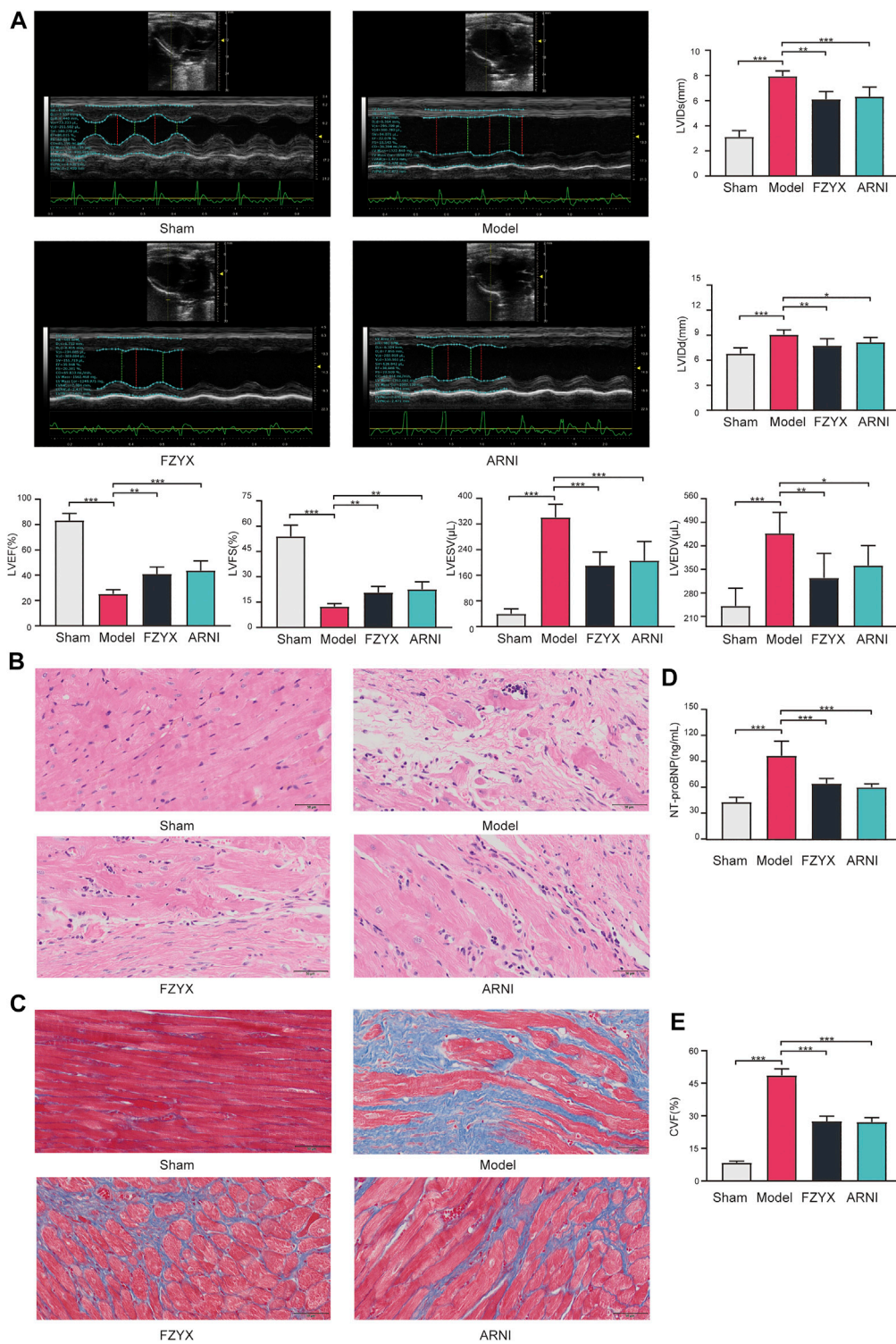


FIGURE 6 Effects of FZYX on cardiac function and structural alterations in HF model rats. **(A)** Echocardiographic results ($n = 5$). Statistical analysis was performed including the LVEF, LVFS, LVESV, LVEDV, LVIDs and LVIDd. **(B)** HE staining. **(C)** Masson's staining. **(D)** NT-proBNP ($n = 5$). **(E)** CVF ($n = 5$) * $p < 0.05$, ** $p < 0.01$, *** $p < 0.001$ vs. controls.

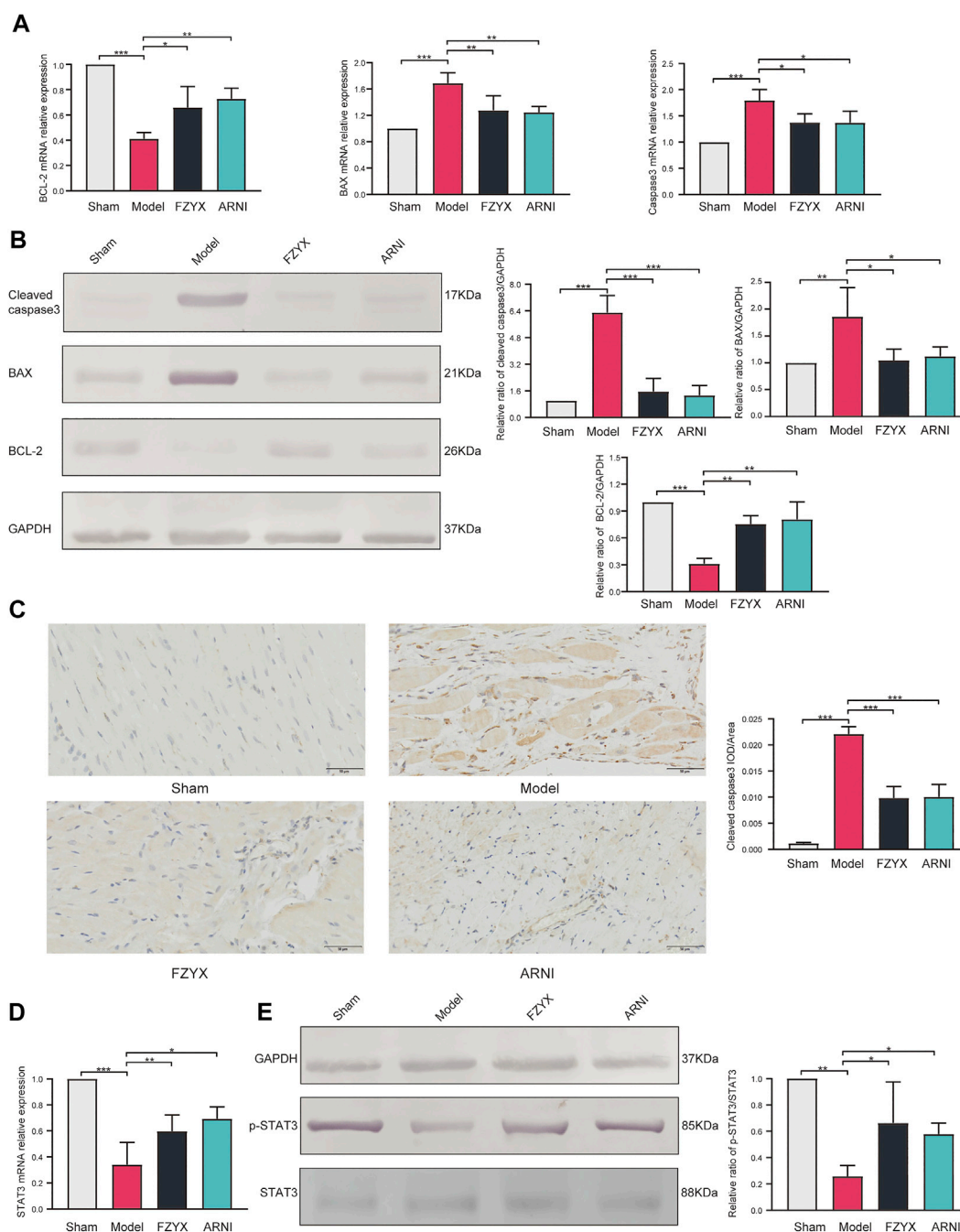


FIGURE 7 Regulation of apoptosis and STAT3 by FZYX. **(A)** mRNA expression levels of BCL-2, BAX and Caspase-3 ($n = 3$). **(B)** Protein abundance of BCL-2, BAX and Caspase-3 ($n = 3$). **(C)** immunohistochemical analysis of Caspase-3 ($n = 5$). **(D)** mRNA expression levels of STAT3 ($n = 3$). **(E)** Protein abundance of pSTAT3 and STAT3 ($n = 3$). * $p < 0.05$, ** $p < 0.01$, *** $p < 0.001$ vs. controls.

database to collect and screen the active components of FZYX, and finally obtained 143 compounds. Some of these ingredients exert their cardioprotective effects through known mechanisms determined by *in vitro* and *in vivo* experiments. Kaempferol, a natural flavonoid compound,

possesses anti-inflammatory and antioxidant activities (Devi et al., 2015; Yeung et al., 2019). On the one hand, Kaempferol can stimulate the notch receptor 1 (Notch1)/phosphatase and tensin homolog (PTEN)/protein kinase B (AKT) signalling pathway, activate sirtuin 1 (SIRT1), inhibit

the MAPK signalling pathway to reduce myocardial ischemic injury (Guo et al., 2015; Suchal et al., 2016; Huang and Qi, 2020); on the other hand, it can inhibit cardiac hypertrophy via regulation of the apoptosis signal-regulating kinase1 (ASK1)/MAPK signalling pathway (Feng et al., 2017) and modulation of the nuclear factor-kappaB (NF- κ B)/MAPK signalling pathway to inhibit ventricular fibrosis (Du et al., 2019). Salidroside is the main active ingredient of *Rhodiola crenulata* (Hook.f.et Thoms.) H. Ohba, and has good biological activity for the treatment of cardiovascular and metabolic diseases (Zhao et al., 2021). Salidroside can modulate disordered homeostasis of energy and lipid metabolism to fight against hypoxia damage in cardiomyocytes (Liao et al., 2020). In addition, salidroside attenuates the pathological process of myocardial remodelling in mice with MI by downregulating the expression levels of tumor necrosis factor-alpha (TNF- α), transforming growth factor- beta 1 (TGF- β 1), interleukin-1beta (IL-1 β) and BAX, and upregulating the expression of BCL-2, vascular endothelial growth factor (VEGF), AKT and endothelial nitric oxide synthase (eNOS) (Chen et al., 2019). Ferulic acid, a phenolic compound with natural antioxidant activity, is able to improve cardiovascular functions and inhibit the pathogenetic cardiovascular disease process (Cheng et al., 2016). Clinical studies have found that ferulic acid is the main active ingredient in the treatment of coronary heart disease (Li et al., 2013). In rat HF models, ferulic acid reduces oxidative stress and inhibits cardiomyocyte apoptosis by activating the nuclear factor erythroid 2-related factor 2 (NRF2) signalling pathway (Zhang et al., 2021). Butylidenephthalide is the main active ingredient of *Angelica sinensis* (Oliv.) Diels (Ying et al., 2013), which can attenuate cardiac fibrosis by regulating the phosphatidylinositol 3-kinase (PI3K)/STAT3-mediated macrophage phenotype in aged rats after MI (Lin et al., 2019). Quercetin (a natural polyphenolic compound) and its metabolites exert cardioprotective effects via antioxidant, anti-inflammatory and molecular pathway modulation in a wide range of experimental models of cardiac injury (Ferenczyova et al., 2020). Quercetin improves cardiomyocyte hypoxic injury by regulating SIRT1/transmembrane BAX inhibitor motif containing 6 (TMBIM6)-related mitophagy and endoplasmic reticulum (ER) stress (Chang et al., 2021). In animal models, quercetin improves myocardial ischemia/reperfusion (I/R)-induced cardiomyocyte apoptosis via SIRT1/peroxisome proliferator-activated receptor gamma coactivator-1 alpha (PGC-1 α) signalling (Tang et al., 2019). Quercetin can inhibit myocardial hypertrophy through glycogen synthase kinase-3 (GSK-3) (Chen et al., 2018) and inhibit myocardial fibrosis through the MAPK signalling pathway (Min et al., 2019). Ligustilide, a natural benzoquinone derivative, protects vascular endothelial cells and rescues high fat diet-induced

atherosclerosis by activating multiple NRF2 downstream genes (Zhu et al., 2019).

After obtaining the active ingredients of FZYX, we used SwissTargetPrediction to predict the target of the drug. The results were intersected with the DEGs of IHD-induced HF, and 37 intersection genes were finally obtained. PPI and functional enrichment analyses were performed on these 37 genes to discover the underlying mechanisms. Based on the results of PPI and enrichment analysis, STAT3 and apoptosis were selected as the key roles of FZYX prescription for subsequent studies. The results of molecular docking also showed that the main components of FZYX and STAT3 had good binding activity. STAT3 can affect cell-to-cell communication, signal transduction and gene transcription. A large number of previous studies have confirmed the role of STAT3 in tumours (Tolomeo and Cascio, 2021). In recent years, many studies have found that STAT3 and its related signalling pathways also play a key regulatory role in the cardiovascular system, such as IHD, HF and myocardial hypertrophy (Hilfiker-Kleiner et al., 2005). Phosphorylation and activation of STAT3 have been widely observed in the heart after ischemia or Ischemia/Reperfusion I/R (Zhao et al., 2019; Takahashi et al., 2020). Western blotting was used to quantify and compare the phosphorylation of various proteins in pig left ventricular samples in a large number of I/R experiments, and the results showed that STAT3 is a common pathway for ischemic regulation (Kleinbongard et al., 2018). After subacute MI, downregulation and continuous impaired activation of STAT3 can lead to poor remodelling and HF (Hilfiker-Kleiner et al., 2010). One study infected myocardial-specific STAT3 knockout mice with tamoxifen for 14 consecutive days from the 11th day after MI to establish a subacute MI (STAT3 iCKO) mouse model. Results showed that the mortality of STAT3 iCKO mice was increased, myocardial fibrosis was significantly worsened, and heart function deteriorated (Enomoto et al., 2015). STAT3 also plays a role in macrophage-mediated post-MI repair, mainly through the IL10-STAT3-Galectin 3 axis promoting osteopontin-mediated generation of reparative macrophages, which promote MI by stimulating fibrosis and the clearance of apoptotic cells (Shirakawa et al., 2018). These results indicate that moderately active STAT3 in the heart endows resistance to cardiac remodelling during myocardial ischemia injury, and participates in the protective effect of various interventions on myocardial ischemia.

Apoptosis is the process of programmed cell death, which is primarily mediated by the death receptor pathway and the mitochondrial apoptosis pathway (Zhang et al., 2019). Apoptosis is an important cause of myocardial injury in patients with acute MI, and is involved in the subsequent development of ventricular remodelling and HF (Terिंगova and Tousek, 2017). Activation of STAT3 has been shown to reduce myocardial cell apoptosis during myocardial ischemia

injury. STAT3-deficient mice have increased susceptibility to myocardial I/R injury and infarction, increased cardiac apoptosis, increased infarct size, and decreased cardiac functions and survival rate (Hilfiker-Kleiner et al., 2004). Activated STAT3 binds to cyclophilin D, a matrix protein that promotes mitochondrial permeability transition pore (MPTP) opening when bound to the mitochondrial inner membrane, and inhibits MPTP opening (Boengler et al., 2010). MPTP opening leads to the release of apoptotic factors, such as cytochrome C (Cyt C), into the cytoplasm (Cavalcante et al., 2019). Cyt C then interacts with apoptotic protease activating factor-1 (Apaf-1) and forms an apoptotic complex with the assistance of adenosine triphosphate (ATP) and deoxyadenosine triphosphate (dATP). The apoptotic complex recruits and activates Pro-Caspase-9 to form cleaved-Caspase-9, which activates Caspase-3 and Caspase-7, triggering the Caspase cascade reaction, finally leading to cell apoptosis (Zhu et al., 2021).

To test whether FZYX exerts cardiac protective effects through apoptosis and STAT3, we performed animal experiments. The results of echocardiography and NT-proBNP showed that FZYX could improve cardiac function in the HF model. The qRT-PCR and western blotting showed that FZYX could increase the expression of BCL-2 and decrease the expression of BAX, and Caspase-3. The results showed that FZYX had anti-apoptosis ability, which was consistent with the results of enrichment analysis. We also tested the effect of FZYX on STAT3 expression. The qRT-PCR showed that FZYX could upregulate STAT3 mRNA expression levels, and western blotting showed that the pSTAT3:STAT3 ratio was increased, indicating that the anti-apoptotic mechanism of FZYX might be related to STAT3.

5 Conclusion

In summary, this study systematically investigated the mechanism of FZYX in the treatment of HF through a combination of network pharmacology and experimental validation. Network pharmacology revealed that FZYX contains various active components that exert cardioprotective effects through multiple targets and signalling pathways. STAT3 may be the core factor of FZYX action, and the anti-apoptotic activity may be one of the most important effects of FZYX in protecting cardiac function. In addition, we verified the effect of FZYX on STAT3 expression and its anti-apoptotic effects in a rat model of ischemic HF.

6 Limitations

In this study, we only focused on the apoptotic pathway and STAT3, and did not fully utilize the results derived from network pharmacology. Second, this study is only a preliminary exploratory study, and the inhibitor group is not designed. In

our subsequent study, a more reasonable design will be carried out to increase the reliability of the conclusion.

Data availability statement

The original contributions presented in the study are included in the article/Supplementary Material, further inquiries can be directed to the corresponding author.

Ethics statement

The animal study was reviewed and approved by the ethics committee of Xiyuan Hospital.

Author contributions

AW: Conceptualization, methodology, software, formal analysis, investigation, resources, data curation, writing—original draft, visualization. WZ: Conceptualization, methodology, writing—review and editing. KY: Conceptualization, methodology, writing—review and editing. LG: Software, data curation. FG: Formal analysis, visualization. JC: Investigation, resources. YW: Validation, writing—review and editing. XM: Conceptualization, writing—review and editing, supervision, project administration.

Funding

This work was supported by the Capital Clinical Characteristic Application Research (No. Z181100001718128).

Acknowledgments

We would like to acknowledge Hong Liu, Qingzhou Station Primary School, Weifang, China for writing assistance.

Conflict of interest

The authors declare that the research was conducted in the absence of any commercial or financial relationships that could be construed as a potential conflict of interest.

Publisher's note

All claims expressed in this article are solely those of the authors and do not necessarily represent those of

their affiliated organizations, or those of the publisher, the editors and the reviewers. Any product that may be evaluated in this article, or claim that may be made by its manufacturer, is not guaranteed or endorsed by the publisher.

References

- Benjamin, E. J., Muntner, P., Alonso, A., Bittencourt, M. S., Callaway, C. W., Carson, A. P., et al. (2019). Heart disease and stroke statistics-2019 update: A report from the American heart association. *Circulation* 139 (10), 56–528. doi:10.1161/CIR.0000000000000659
- Boengler, K., Hilfiker-Kleiner, D., and HeuschSchulz, G. R. (2010). Inhibition of permeability transition pore opening by mitochondrial STAT3 and its role in myocardial ischemia/reperfusion. *Basic Res. Cardiol.* 105 (6), 771–785. doi:10.1007/s00395-010-0124-1
- Burley, S. K., Bhikadiya, C., Bi, C., Bittrich, S., Chen, L., Crichlow, G. V., et al. (2021). RCSB protein Data Bank: Powerful new tools for exploring 3D structures of biological macromolecules for basic and applied research and education in fundamental biology, biomedicine, biotechnology, bioengineering and energy sciences. *Nucleic Acids Res.* 49 (1), D437–D451. doi:10.1093/nar/gkaa1038
- Cavalcante, G. C., Schaana, A. P., Cabral, G. F., Santana-da-Silva, M. N., Pinto, P., Vidal, A. F., et al. (2019). A cell's fate: An overview of the molecular biology and genetics of apoptosis. *Int. J. Mol. Sci.* 20 (17), 4133. doi:10.3390/ijms20174133
- Chang, X., Zhang, T., Meng, Q., Wang, S., Yan, P., Wang, X., et al. (2021). Quercetin improves cardiomyocyte vulnerability to hypoxia by regulating SIRT1/TMBIM6-related mitophagy and endoplasmic reticulum stress. *Oxid. Med. Cell. Longev.* 2021, 5529913. doi:10.1155/2021/5529913
- Chen, K., Rekep, M., Wei, W., Wu, Q., Xue, Q., Li, S., et al. (2018). Quercetin prevents *in vivo* and *in vitro* myocardial hypertrophy through the proteasome-GSK-3 pathway. *Cardiovasc. Drugs Ther.* 32 (1), 5–21. doi:10.1007/s10557-018-6771-4
- Chen, P., Liu, J., Ruan, H., Zhang, M., Wu, P., Yimei, D., et al. (2019). Protective effects of Salidroside on cardiac function in mice with myocardial infarction. *Sci. Rep.* 9 (1), 18127. doi:10.1038/s41598-019-54713-x
- Chen, W. Q., Wang, B., Ding, C. F., Wan, L. Y., Hu, H. M., Lv, B. D., et al. (2021). *In vivo* and *in vitro* protective effects of the Wuzi Yanzong pill against experimental spermatogenesis disorder by promoting germ cell proliferation and suppressing apoptosis. *J. Ethnopharmacol.* 280, 114443. doi:10.1016/j.jep.2021.114443
- Cheng, Y. H., Lin, F. H., Wang, C. Y., Hsiao, C. Y., Chen, H. C., Kuo, H. Y., et al. (2016). Recovery of oxidative stress-induced damage in Cisd2-deficient cardiomyocytes by sustained release of ferulic acid from injectable hydrogel. *Biomaterials* 103, 207–218. doi:10.1016/j.biomaterials.2016.06.060
- Destia, L., Jernberg, T., Lofman, I., Hofman-Bang, C., Hagerman, I., Spaak, J., et al. (2015). Incidence, temporal trends, and prognostic impact of heart failure complicating acute myocardial infarction. The SWEDHEART Registry (Swedish web-system for enhancement and development of evidence-based care in heart disease evaluated according to recommended therapies): A study of 199, 851 patients admitted with index acute myocardial infarctions, 1996 to 2008. *JACC. Heart Fail.* 3 (3), 234–242. doi:10.1016/j.jchf.2014.10.007
- Devi, K. P., Malar, D. S., Nabavi, S. F., Surenda, A., Xiao, J., Nabavi, S. M., et al. (2015). Kaempferol and inflammation: From chemistry to medicine. *Pharmacol. Res.* 99, 1–10. doi:10.1016/j.phrs.2015.05.002
- Disease, G. B. D. (2018). Injury, I. Prevalence, CGlobal, regional, and national incidence, prevalence, and years lived with disability for 354 diseases and injuries for 195 countries and territories, 1990-2017: A systematic analysis for the global burden of disease study 2017. *Lancet* 392 (10159), 1789–1858. doi:10.1016/S0140-6736(18)32279-7
- Du, Y., Han, J., Zhang, H., Xu, J., and JiangGe, L. W. (2019). Kaempferol prevents against ang II-induced cardiac remodeling through attenuating ang II-induced inflammation and oxidative stress. *J. Cardiovasc. Pharmacol.* 74 (4), 326–335. doi:10.1097/FJC.0000000000000713
- Enomoto, D., Obana, M., Miyawaki, A., Maeda, M., and NakayamaFujio, H. Y. (2015). Cardiac-specific ablation of the STAT3 gene in the subacute phase of myocardial infarction exacerbated cardiac remodeling. *Am. J. Physiol. Heart Circ. Physiol.* 309 (3), H471–H480. doi:10.1152/ajpheart.00730.2014
- Feng, H., Cao, J., and ZhangWang, G. Y. (2017). Kaempferol attenuates cardiac hypertrophy via regulation of ASK1/MAPK signaling pathway and oxidative stress. *Planta Med.* 83 (10), 837–845. doi:10.1055/s-0043-103415
- Ferenczyova, K., and KalocayovaBartekova, B. M. (2020). Potential implications of quercetin and its derivatives in cardioprotection. *Int. J. Mol. Sci.* 21 (5), E1585. doi:10.3390/ijms21051585
- Gan, X. T., Ettinger, G., Huang, C. X., Burton, J. P., Haist, J. V., Rajapurohitam, V., et al. (2014). Probiotic administration attenuates myocardial hypertrophy and heart failure after myocardial infarction in the rat. *Circ. Heart Fail.* 7 (3), 491–499. doi:10.1161/CIRCHEARTFAILURE.113.000978
- Gosak, M., Markovic, R., Dolensek, J., Slak Rupnik, M., Marhl, M., Stozar, A., et al. (2018). Network science of biological systems at different scales: A review. *Phys. Life Rev.* 24, 118–135. doi:10.1016/j.plrev.2017.11.003
- Guo, L. J. (2018). *Clinical and metabolomic study on the treatment of heart failure by blood ultrafiltration with Yiqi Fuzheng therapy. dissertation.* Beijing: Beijing University of Chinese Medicine.
- Guo, Z., Liao, Z., Huang, L., Liu, D., and YinHe, D. M. (2015). Kaempferol protects cardiomyocytes against anoxia/reoxygenation injury via mitochondrial pathway mediated by SIRT1. *Eur. J. Pharmacol.* 761, 245–253. doi:10.1016/j.ejphar.2015.05.056
- Heusch, G. (2020). Myocardial ischaemia-reperfusion injury and cardioprotection in perspective. *Nat. Rev. Cardiol.* 17 (12), 773–789. doi:10.1038/s41569-020-0403-y
- Hilfiker-Kleiner, D., Hilfiker, A., Fuchs, M., Kaminski, K., Schaefer, A., Schieffer, B., et al. (2004). Signal transducer and activator of transcription 3 is required for myocardial capillary growth, control of interstitial matrix deposition, and heart protection from ischemic injury. *Circ. Res.* 95 (2), 187–195. doi:10.1161/01.RES.0000134921.50377.61
- Hilfiker-Kleiner, D., and HilfikerDrexler, A. H. (2005). Many good reasons to have STAT3 in the heart. *Pharmacol. Ther.* 107 (1), 131–137. doi:10.1016/j.pharmthera.2005.02.003
- Hilfiker-Kleiner, D., Shukla, P., Klein, G., Schaefer, A., Stapel, B., Hoch, M., et al. (2010). Continuous glycoprotein-130-mediated signal transducer and activator of transcription-3 activation promotes inflammation, left ventricular rupture, and adverse outcome in subacute myocardial infarction. *Circulation* 122 (2), 145–155. doi:10.1161/CIRCULATIONAHA.109.933127
- Huang, J. H., Huang, X. H., Chen, Z. Y., and ZhengSun, Q. S. R. Y. (2004). Dose conversion among different animals and healthy volunteers in pharmacological study. *Zhongguo Lin. chuang yao li xue yu zhi liao xue* 9 (09), 1069–1072.
- HuangQi, J. Z. (2020). MiR-21 mediates the protection of kaempferol against hypoxia/reoxygenation-induced cardiomyocyte injury via promoting Notch1/PTEN/AKT signaling pathway. *PLoS one* 15 (11), e0241007. doi:10.1371/journal.pone.0241007
- Kibble, M., Saarinen, N., Tang, J., Wennerberg, K., and MakelaAittokallio, S. T. (2015). Network pharmacology applications to map the unexplored target space and therapeutic potential of natural products. *Nat. Prod. Rep.* 32 (8), 1249–1266. doi:10.1039/c5np00005j

Supplementary material

The Supplementary Material for this article can be found online at: <https://www.frontiersin.org/articles/10.3389/fphar.2022.1004929/full#supplementary-material>

- Kleinbongard, P., Skyschally, A., Gent, S., and PeschHeusch, M. G. (2018). STAT3 as a common signal of ischemic conditioning: A lesson on "rigor and reproducibility" in preclinical studies on cardioprotection. *Basic Res. Cardiol.* 113 (1), 3. doi:10.1007/s00395-017-0660-z
- Li, Y. H., Huang, X., Wang, Y., Fan, R., Zhang, H. M., Ren, P., et al. (2013). Pharmacokinetic comparison of the vasorelaxant compound ferulic acid following the administration of Guanxin II to healthy volunteers and patients with angina pectoris. *Exp. Ther. Med.* 6 (5), 1283–1289. doi:10.3892/etm.2013.1302
- Liao, W., Liu, J., Wang, S., Xue, Z., Zheng, F., Feng, F., et al. (2020). Metabolic profiling reveals that salidroside antagonizes hypoxic injury via modulating energy and lipid metabolism in cardiomyocytes. *Biomed. Pharmacother.* 122, 109700. doi:10.1016/j.biopha.2019.109700
- Lin, C. C., Chen, S. Y., Lien, H. Y., and LinLee, S. Z. T. M. (2019). Targeting the PI3K/STAT3 axis modulates age-related differences in macrophage phenotype in rats with myocardial infarction. *J. Cell. Mol. Med.* 23 (9), 6378–6392. doi:10.1111/jcmm.14526
- Lindsey, M. L., Bolli, R., Canty, J. M., Jr., Du, X. J., Frangogiannis, N. G., Frantz, S., et al. (2018). Guidelines for experimental models of myocardial ischemia and infarction. *Am. J. Physiol. Heart Circ. Physiol.* 314 (4), H812–H838–H838. doi:10.1152/ajpheart.00335.2017
- Liu, Z., Guo, F., Wang, Y., Li, C., Zhang, X., Li, H., et al. (2016). BATMAN-TCM: A Bioinformatics analysis tool for molecular mechanism of traditional Chinese medicine. *Sci. Rep.* 6, 21146. doi:10.1038/srep21146
- LiZhang, S. B. (2013). Traditional Chinese medicine network pharmacology: Theory, methodology and application. *Chin. J. Nat. Med.* 11 (2), 110–120. doi:10.1016/S1875-5364(13)60037-0
- Martin, A., Ochagavia, M. E., Rabasa, L. C., Miranda, J., and Fernandez-de-CossioBringas, J. R. (2010). BisoGenet: A new tool for gene network building, visualization and analysis. *BMC Bioinforma.* 11, 91. doi:10.1186/1471-2105-11-91
- McDonagh, T. A., Metra, M., Adamo, M., Gardner, R. S., Baumbach, A., Bohm, M., et al. (2021). 2021 ESC Guidelines for the diagnosis and treatment of acute and chronic heart failure. *Eur. Heart J.* 42 (36), 3599–3726. doi:10.1093/eurheartj/ehab368
- Min, Z., Yangchun, L., and YuquanChangying, W. Z. (2019). Quercetin inhibition of myocardial fibrosis through regulating MAPK signaling pathway via ROS. *Pak. J. Pharm. Sci.* 32 (3), 1355–1359.
- Moors, B. H. M. (2020). Shortcuts for faster image creation in PyMOL. *Protein Sci.* 29 (1), 268–276. doi:10.1002/pro.3781
- Pfau, D., Thorn, S. L., Zhang, J., Mikush, N., Renaud, J. M., Klein, R., et al. (2019). Angiotensin receptor neprilysin inhibitor attenuates myocardial remodeling and improves infarct perfusion in experimental heart failure. *Sci. Rep.* 9 (1), 5791. doi:10.1038/s41598-019-42113-0
- Schneider, C. A., and RasbandEliceiri, W. S. K. W. (2012). NIH image to ImageJ: 25 years of image analysis. *Nat. Methods* 9 (7), 671–675. doi:10.1038/nmeth.2089
- Shannon, P., Markiel, A., Ozier, O., Baliga, N. S., Wang, J. T., Ramage, D., et al. (2003). Cytoscape: A software environment for integrated models of biomolecular interaction networks. *Genome Res.* 13 (11), 2498–2504. doi:10.1101/gr.1239303
- Shirakawa, K., Endo, J., Kataoka, M., Katsumata, Y., Yoshida, N., Yamamoto, T., et al. (2018). IL (Interleukin)-10-STAT3-Galectin-3 Axis is essential for osteopontin-producing reparative macrophage polarization after myocardial infarction. *Circulation* 138 (18), 2021–2035. doi:10.1161/CIRCULATIONAHA.118.035047
- Suchal, K., Malik, S., Gamad, N., Malhotra, R. K., Goyal, S. N., Chaudhary, U., et al. (2016). Kaempferol attenuates myocardial ischemic injury via inhibition of MAPK signaling pathway in experimental model of myocardial ischemia-reperfusion injury. *Oxid. Med. Cell. Longev.* 2016, 7580731. doi:10.1155/2016/7580731
- Sunagawa, Y., Sono, S., Katanasaka, Y., Funamoto, M., Hirano, S., Miyazaki, Y., et al. (2014). Optimal dose-setting study of curcumin for improvement of left ventricular systolic function after myocardial infarction in rats. *J. Pharmacol. Sci.* 126 (4), 329–336. doi:10.1254/jphs.14151FP
- Takahashi, J., Yamamoto, M., Yasukawa, H., Nohara, S., Nagata, T., Shimozono, K., et al. (2020). Interleukin-22 directly activates myocardial STAT3 (signal transducer and activator of transcription-3) signaling pathway and prevents myocardial ischemia reperfusion injury. *J. Am. Heart Assoc.* 9 (8), e014814. doi:10.1161/JAHA.119.014814
- Tang, J., Lu, L., Liu, Y., Ma, J., Yang, L., Li, L., et al. (2019). Quercetin improve ischemia/reperfusion-induced cardiomyocyte apoptosis *in vitro* and *in vivo* study via SIRT1/PGC-1 α signaling. *J. Cell. Biochem.* 120 (6), 9747–9757. doi:10.1002/jcb.28255
- TangHuang, W. H. W. Y. (2013). Cardiotoxic modulation in heart failure: Insights from traditional Chinese medicine. *J. Am. Coll. Cardiol.* 62 (12), 1073–1074. doi:10.1016/j.jacc.2013.05.028
- TeringovaTousek, E. P. (2017). Apoptosis in ischemic heart disease. *J. Transl. Med.* 15 (1), 87. doi:10.1186/s12967-017-1191-y
- TolomeoCascio, M. A. (2021). The multifaced role of STAT3 in cancer and its implication for anticancer therapy. *Int. J. Mol. Sci.* 22 (2), E603. doi:10.3390/ijms22020603
- TrottOlson, O. A. J. (2010). AutoDock vina: Improving the speed and accuracy of docking with a new scoring function, efficient optimization, and multithreading. *J. Comput. Chem.* 31 (2), 455–461. doi:10.1002/jcc.21334
- Vaskova, E., Ikeda, G., Tada, Y., Wahlquist, C., and MercolaYang, M. P. C. (2020). Sacubitril/valsartan improves cardiac function and decreases myocardial fibrosis via downregulation of exosomal miR-181a in a rodent chronic myocardial infarction model. *J. Am. Heart Assoc.* 9 (13), e015640. doi:10.1161/JAHA.119.015640
- Wang, Y., Fu, M., Wang, J., Zhang, J., Han, X., Song, Y., et al. (2020). Qiliqiangxin improves cardiac function through regulating energy metabolism via HIF-1 α -Dependent and independent mechanisms in heart failure rats after acute myocardial infarction. *Biomed. Res. Int.* 2020, 1276195. doi:10.1155/2020/1276195
- Xu, H. Y., Zhang, Y. Q., Liu, Z. M., Chen, T., Lv, C. Y., Tang, S. H., et al. (2019). EtcM: An encyclopaedia of traditional Chinese medicine. *Nucleic Acids Res.* 47 (D1), D976–D982. doi:10.1093/nar/gky987
- Yeung, A. W. K., Tzvetkov, N. T., El-Tawil, O. S., Bungau, S. G., and Abdel-DaimAtanasov, M. M. A. G. (2019). Antioxidants: Scientific literature landscape analysis. *Oxid. Med. Cell. Longev.* 2019, 8278454. doi:10.1155/2019/8278454
- Ying, L., Si-Wang, W., and Hong-HaiWei, T. C. (2013). Simultaneous quantification of six main active constituents in Chinese Angelica by high-performance liquid chromatography with photodiode array detector. *Pharmacogn. Mag.* 9 (34), 114–119. doi:10.4103/0973-1296.111255
- Zhang, J., Liu, D., and ZhangZhang, M. Y. (2019). Programmed necrosis in cardiomyocytes: Mitochondria, death receptors and beyond. *Br. J. Pharmacol.* 176 (22), 4319–4339. doi:10.1111/bph.14363
- Zhang, X. J., Cui, Z. H., Zhao, Y. X., He, T. T., and WangLiang, L. X. W. (2021). Ferulic acid ameliorates isoproterenol-induced heart failure by decreasing oxidative stress and inhibiting cardiocyte apoptosis via activating Nrf2 signaling pathway in rats. *Biol. Pharm. Bull.* 44 (3), 396–403. doi:10.1248/bpb.b20-00783
- Zhang, Y., Zhang, J., Butler, J., Yang, X., Xie, P., Guo, D., et al. (2017). Contemporary epidemiology, management, and outcomes of patients hospitalized for heart failure in China: Results from the China heart failure (China-HF) Registry. *J. Card. Fail.* 23 (12), 868–875. doi:10.1016/j.cardfail.2017.09.014
- Zhao, C. C., Wu, X. Y., Yi, H., and ChenFan, R. G. (2021). The therapeutic effects and mechanisms of salidroside on cardiovascular and metabolic diseases: An updated review. *Chem. Biodivers.* 18 (7), e2100033. doi:10.1002/cbdv.202100033
- Zhao, C., Zhang, B., Jiang, J., and WangWu, Y. Y. (2019). Up-regulation of ANXA1 suppresses polymorphonuclear neutrophil infiltration and myeloperoxidase activity by activating STAT3 signaling pathway in rat models of myocardial ischemia-reperfusion injury. *Cell. Signal.* 62, 109325. doi:10.1016/j.cellsig.2019.05.010
- Zheng, Y. (2020). *Clinical and targeted metabolomics study of Chinese medicine combined with blood ultrafiltration in the treatment of heart failure dissertation*. Beijing: Beijing University of Chinese Medicine.
- Zhu, H., Toan, S., and MuiZhou, D. H. (2021). Mitochondrial quality surveillance as a therapeutic target in myocardial infarction. *Acta Physiol. (Oxf).* 231 (3), e13590. doi:10.1111/apha.13590
- Zhu, Y., Zhang, Y., Huang, X., Xie, Y., Qu, Y., Long, H., et al. (2019). Z-Ligustilide protects vascular endothelial cells from oxidative stress and rescues high fat diet-induced atherosclerosis by activating multiple NRF2 downstream genes. *Atherosclerosis* 284, 110–120. doi:10.1016/j.atherosclerosis.2019.02.010

Glossary

- AGE** Advanced glycation end-product
- AKT** Protein kinase B
- ANOVA** One-way analysis of variance
- Apaf-1** Apoptotic protease activating factor-1
- ARNI** Angiotensin receptor neprilysin inhibitors
- ASK1** Apoptosis signal-regulating kinase1
- ATP** Adenosine triphosphate
- BAX** Pro-apoptotic BCL-2 associated X
- BC** Between centrality
- BCA** Bicinchoninic acid
- BCL-2** B cell lymphoma-2
- BP** Biological process
- CC** Cellular component
- CCND1** Cyclin D1
- cGMP** Cyclic guanosine monophosphate
- CVF** Collagen volume fraction
- Cyt C** Cytochrome C
- DAB** 3,3'-diaminobenzidine
- dATP** Deoxyadenosine triphosphate
- DC** Degree centrality
- DCM** idiopathic dilated cardiomyopathy
- DEGs** differentially expressed genes
- DEPC** Diethyl pyrocarbonate
- ELISA** Enzyme-linked immunosorbent assay
- eNOS** Endothelial nitric oxide synthase
- ER** Endoplasmic reticulum
- FC** Fold change
- Fc epsilon RI**, High-affinity receptors for immunoglobulin E
- FOXO** Forkhead box O
- FZYX** Fuzheng Yangxin Recipe
- GEO** Gene expression omnibus
- GO** Gene Ontology
- GSK-3** Glycogen synthase kinase-3
- HE** Hematoxylin-eosin
- HF** Heart failure
- I/R** Ischemia/reperfusion
- IHD** Ischemic heart disease
- IL-1 β** Interleukin-1beta
- IOD** Integrated option density
- KEGG** Kyoto Encyclopedia of Genes and Genomes
- LC** Liquid chromatography
- LSD** Least significant difference
- LVEDV** Left ventricular end-diastolic volume
- LVEF** Left ventricular ejection fraction
- LVESV** Left ventricular end-systolic volume
- LVFS** Left ventricular fractional shortening
- LVIDd** Left ventricular internal dimension end-diastolic
- LVIDs** Left ventricular internal dimension end-systolic
- MAP2K1** Mitogen-activated protein kinase kinase 1
- MAPK** Mitogen-activated protein kinase
- MF** Molecular function
- MI** Myocardial infarction
- MPTP** Mitochondrial permeability transition pore
- MS** Mass spectrometry
- NF** Non-failing
- NF- κ B** Nuclear factor-kappaB
- Notch1** Notch receptor 1
- NRF2** Nuclear factor erythroid 2-related factor 2
- NT-proBNP** N-terminal pro-B-type natriuretic peptide
- PGC-1 α** Peroxisome proliferator-activated receptor gamma coactivator-1 alpha
- PI3K** Phosphatidylinositol 3-kinase
- PKG** Protein kinase G
- PPI** Protein-protein interaction
- PTEN** Phosphatase and tensin homolog
- PVDF** Polyvinylidene fluoride
- qRT-PCR** Quantitative real-time PCR
- RAGE** Receptor for AGE
- SDS-PAGE** Sodium dodecyl sulphate polyacrylamide gel electrophoresis
- SIRT1** Sirtuin 1
- STAT3** Signal transducer and activator of transcription 3
- SMOC2** Secreted modular calcium-binding protein 2
- TBST** Tris Buffered Saline with Tween 20
- TCM** Traditional Chinese medicine
- TGF- β 1** Transforming growth factor- beta 1
- TMBIM6** Transmembrane BAX inhibitor motif containing 6
- TNF- α** Tumor necrosis factor-alpha
- VEGF** Vascular endothelial growth factor
- VSIG4** V-set and immunoglobulin domain containing 4